Folding of the SAM Aptamer is Determined by the Formation of a K-turn-dependent Pseudoknot†

Benoit Heppell and Daniel A. Lafontaine*

Département de biologie, Faculté des sciences, Université de Sherbrooke, Sherbrooke, Québec, Canada J1K 2R1

Received June 13, 2007; Revised Manuscript Received November 12, 2007

ABSTRACT: The *S*-adenosylmethionine (SAM) riboswitch is one of the most recurrent riboswitches found in bacteria and has three known different natural aptamers. The *Bacillus subtilis yitJ* SAM riboswitch aptamer is organized around a four-way junction which is characterized by the presence of a pseudoknot and a K-turn motif. By replacing the adenine involved in a Watson−Crick base pair at position 138 in the core region of the aptamer with the fluorescent analogue 2-aminopurine (2AP), we show that the ligand-induced reorganization of the aptamer strongly attenuates 2AP fluorescence. The fluorescence quenching process is specific to SAM on the basis of the observation that the structural analogue *S*-adenosylhomocysteine does not promote a similar effect. We find that the pseudoknot is important for the reorganization of the core domain and that the K-turn motif also has a marked influence on the core domain reorganization, most probably through its important role in pseudoknot formation. Finally, we show that SAM riboswitch ligand binding is facilitated by the L7Ae K-turn binding protein, which suggests that K-turn motifs may be protein anchor sites used by riboswitches to promote RNA folding.

The *S*-adenosylmethionine (SAM) metabolite is an essential coenzyme in all organisms that is directly synthesized from methionine by SAM synthetase and also serves as a source of methyl groups for protein and nucleic acid modification (*1*). Genes regulated by SAM riboswitches are related to sulfur metabolism, including those that are involved in the biosynthesis of cysteine, methionine, and SAM (*2*). In addition, it has been shown that overexpression of SAM synthetase leads to methionine deficiency in *Bacillus subtilis*, suggesting that SAM rather than methionine is an effector molecule of methionine biosynthesis in vivo (*3*). Recently, a series of in vitro studies using different techniques have shown that SAM exerts its regulatory control via the action of a SAM-dependent riboswitch (*4*−*6*). SAM riboswitches are the most frequently occurring riboswitches in Gram-positive organisms, and 26 genes included in 11 transcriptional units are controlled by SAM riboswitches in *B. subtilis* (*2*, *4*−*9*).

SAM riboswitches are classified into three structurally different families, in which class I is characterized by the presence of a single four-way junction (*2*, *4*−*7*). The core of the *yitJ* SAM binding aptamer (S box) comprises four helices (P1−P4) and has been shown to induce transcription attenuation in vitro upon SAM binding, where the P1 stem is formed in the presence of the ligand (*4*, *6*, *7*) (Figure 1A). The global architecture of the S box is established through an intricate set of tertiary interactions occurring among the L2, J3/4, and J1/4 regions, as observed in the crystal structure (*10*). As a result, the structure of the RNA is organized around two sets of coaxially stacked helices, P1−P4 and P2−P3, which are oriented relative to each other with an angle of ∼70° (Figure 1B). The ligand binding site is formed by minor grooves of P1 and P3 helices, in which the adenine ring of SAM interacts with the junction-proximal bulge of the P3 stem. The methionine moiety of the SAM ligand is involved in interactions with the J1/2 single strand, consistent with previous in-line probing experiments (*6*). In addition, the crystal structure also shows a K-turn structure, originally called the GA motif (*11*), that is located in the P2 helical region. This motif occurs in several locations in the 23S rRNA of *Haloarcula marismortui* (*12*) and in the 16S rRNA of *Thermus thermophilus* (*13*). The overall structure of the K-turn motif is conserved to a high degree (*14*). The K-turn motif is characterized by the presence of an asymmetric loop, a protruded nucleotide, two tandem GA pairs, and a sharp bend in the phosphate backbone (*14*, *15*). A coaxial base stack constitutes a central hydrophobic core for organizing the K-turn RNA structure, a folding principle reminiscent of globular proteins (*16*). It was recently found that the coaxial base stack can be perturbed by introducing a single A to C mutation, thereby completely inhibiting the adoption of the kinked structure (*17*). Also, given that most K-turn representatives in the ribosome are involved in protein binding, the K-turn is an important protein recognition element. While most ribosomal RNA K-turn motifs serve as protein-anchoring points, they are also important as scaffolding elements for building complex RNA architectures (*14*). In the case of the SAM riboswitch, its K-turn motif provides correct orientation to the P2 stem−loop to form a structurally important pseudoknot with the J3/4 single-strand region (*10*). However, although both the pseudoknot and the K-turn motif have been shown to be important for SAM

† This work was supported by the National Sciences and Engineering Research Council of Canada (NSERC). B.H. is supported by an NSERC studentship.

* To whom correspondence should be addressed. Phone: (819) 821-8000, ext 65011. Fax: (819) 821-8049. E-mail: Daniel.Lafontaine@USherbrooke.ca.

10.1021/bi701164y CCC: $40.75
Published on Web 01/19/2008

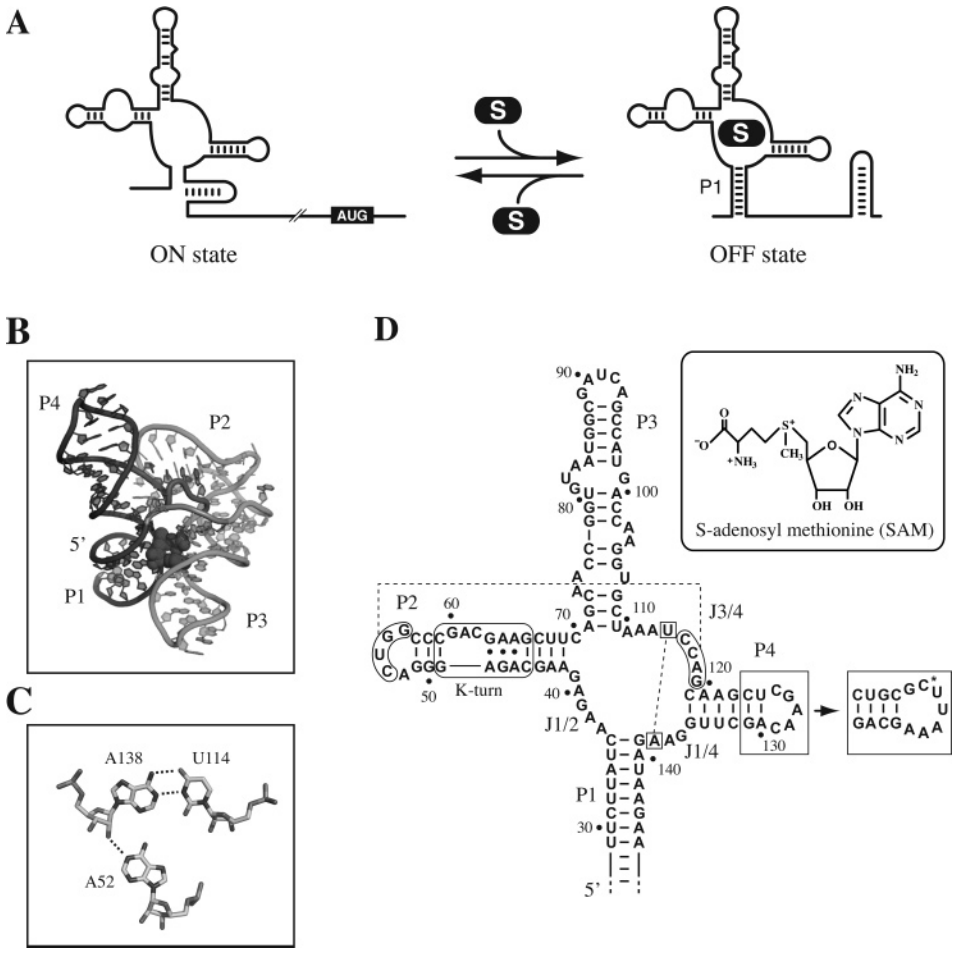

FIGURE 1: *B. subtilis yitJ* SAM riboswitch. (A) Schematic representing the ligand-induced SAM riboswitch premature transcription termination. Structures in the absence (ON state) and in the presence (OFF state) of SAM (S) are shown. Please note that the P1 stem is only formed in presence of SAM ligand. (B) Representation of a front view of the three-dimensional structure of the SAM aptamer (adapted from ref *10*). The ligand is located between the P1 and P3 stems and is shown as spheres. The 5′ extremity of the aptamer is shown. While the P1 and P4 helices are shown in black, the P2 and P3 helices are shown in gray. This figure was made using PyMOL (*61*). (C) Molecular interactions involving the base triple A138, U114, and A52. Hydrogen bonds are shown as dashed lines (adapted from ref *10*). (D) Secondary structure of the SAM aptamer construct used in this study. Nucleotides involved in the pseudoknot and in the U114−A138 base pairing are circled and boxed, respectively. The K-turn motif is shown in the P2 helical domain. P1 and P4 stem sequences have been altered to increase RNA ligation (see the Materials and Methods), and the ligation site is marked by an asterisk. The P4 stem−loop sequence used in this study is shown in a box. Sequence numbering is according to refs *4* and *6*. The chemical structure of *S*-adenosylmethionine is shown in the inset.

riboswitch regulation (*7*, *11*), no experimental data are currently available on the influence of both structures on the folding of the SAM binding domain, which is the core of the aptamer, and its functional importance on riboswitch regulation.

The recently solved crystal structure of the SAM aptamer bound to its cognate ligand shows that U114, located in the J3/4 region, is involved in a Watson−Crick base pair with A138 (*10*) (Figure 1C). In addition, the 2′-OH of A138 is involved with the N1 position of A52. Given that A138 is located in the core region, we speculated that its local environment should be influenced by a SAM-dependent reorganization of the aptamer as shown by in-line probing assays (*6*). A 2-aminopurine (2AP) fluorescent reporter was thus substituted for the adenine located at position 138, and the variation in the 2AP fluorescence intensity was used as a measure of structural changes in its local environment (Figure 1D). 2AP is a strongly fluorescent base that can be selectively excited in the presence of naturally occurring bases (*18*−*23*). Using this fluorescent assay, we studied the folding of the SAM aptamer as a function of metal ions and ligands as well as the influence of the pseudoknot and the K-turn motif on the ligand-induced folding of the aptamer. We find that the 2AP local environment is reorganized by SAM binding to the aptamer and that this reorganization is dependent on the formation of the pseudoknot, which is in turn dependent on the correct folding of the K-turn motif. Fluorescence change in 2AP is specific to SAM, given that it is not observed when the *S*-adenosylhomocysteine (SAH) analogue is used. Moreover, we find that the L7Ae protein can form a ribonucleoprotein complex with the K-turn motif present in the aptamer and that ligand binding is facilitated by L7Ae, suggesting that K-turn binding proteins may participate in riboswitch ligand binding activity.

MATERIALS AND METHODS

Purification of DNA Oligonucleotides. Oligonucleotides were purchased from Sigma Genosys (Canada). Oligonucleotides were purified by denaturing polyacrylamide gel electrophoresis, electroeluted into 8 M ammonium acetate, recovered by ethanol precipitation, and dissolved in water.

Synthesis of RNA Molecules. RNA was transcribed from double-stranded DNA template using T7 RNA polymerase (*24*). Templates for transcription were made by recursive PCR from purified synthetic DNA oligonucleotides. In vitro transcription reactions were carried out for a period of 3 h. RNA was purified by denaturing PAGE and recovered as described for DNA oligonucleotides. All transcribed RNA species begin with a 5′-GCG sequence to minimize the 5′-heterogeneity of the RNA population (*25*). 5′-PO_4-2AP-containing RNA oligonucleotides were purchased from Dharmacon (Boulder), deprotected, and purified as described previously (*26*). The SAM-2AP aptamer sequence was based on the *B. subtilis yitJ* variant in which we introduced sequence changes to improve the yield of RNA ligation. Oligonucleotides of the following sequences were used to generate the complete aptamer (all written 5′ to 3′): 5′ strand, GCGCAUAUCCGUUCUUAUCAAGAGAAGCAGAGGGACUGGCCCGACGAAGCUUCAGCAACCGGUGUAAUGGCGAUCAGCCAUGACCAAGGUGCUAAAUCCAGCAAGCUGCGC; 3′ strand, 5′-PO_4-UUAAAGCAGCUUGGA(2AP)GAUAAGAACGGAU.

Mutants were also prepared with the sequence changes indicated in the text. Purified 5′ and 3′ RNA strands were annealed by heating a mixture (molar ratio 1.5:1) to 65 °C in 10 mM Hepes, pH 7.5, 50 mM NaCl, and 10 mM $MgCl_2$ and slowly cooling to 35 °C. T4 RNA ligase (New England BioLabs) was then added to the reaction, and the samples were incubated at 37 °C for 3 h, where typical ligation reaction efficiencies of ∼75% are obtained. Full-length ligated RNA molecules were purified by denaturing polyacrylamide gel electrophoresis and electroelution. The RNA was precipitated with ethanol and redissolved in water. The RNA concentration was measured by absorption of light at 260 nm.

Fluorescence Spectroscopy. Fluorescence spectroscopy was performed on a Quanta Master fluorometer. All data were collected at 10 °C in 10 mM $MgCl_2$, 50 mM Tris−HCl, pH 8.3, and 50 mM NaCl. Excitation for 2AP fluorescence was done at 300 nm to obtain a good separation between the Raman peak and 2AP fluorescence signal. Spectra were corrected for background, and intensities were determined by integrating the data collected over the range 330−420 nm.

2AP fluorescence was determined by monitoring the fluorescence emission of a fixed concentration of fluorescent RNA (300 nM) and titrating with a given ligand. Changes of fluorescence were normalized to the maximum fluorescence measured in the absence of ligand. The binding can thus be described by the binding model

$$\alpha = K_A[\mathrm{SAM}]/(1 + K_A[\mathrm{SAM}])$$

where α is the change in fluorescence intensity and K_A is the association constant. We can calculate an apparent dissociation constant $K_{Dapp} = 1/K_A$ at which the fluorescence transition is 50% complete. All titrations were repeated two or three times, and the reported errors are the standard uncertainties of the data from the best-fit theoretical curves. The standard uncertainty of the measurement is thus assumed to be approximated by the standard deviation of the points from the fitted curve (*27*, *28*). Magnesium titrations were performed as previously described (*22*) using a ligand concentration of 2 μM.

Gel Electrophoresis under Nondenaturing Donditions. Radioactively 5′-^{32}P-labeled RNA (final concentration <1 nM) in 90 mM Tris and 89 mM boric acid, pH ≈ 8.5 (TB buffer), and 10 mM $MgCl_2$ was electrophoresed in 10% acrylamide/bisacrylamide (29:1) gels in TB with 10 mM $MgCl_2$ at 4 °C at 200 V for 24 h. The running buffer was circulated during electrophoresis. Dried gels were exposed to Phosphor Imager screens.

Gel Electrophoresis under Nondenaturing Conditions in the Presence of the L7Ae Protein. Radioactively 5′-^{32}P-labeled RNA samples were prepared in TB buffer, 25 mM NaCl, and 20% glycerol. Purified *Archaeoglobus fulgidus* L7Ae was obtained from David Lilley (*29*) and was added to a concentration of 1 μM where required. Mixtures were incubated on ice for 1 h before being electrophoresed on 10% acrylamide/bisacrylamide (29:1) gels in TB with 25 mM NaCl at 4 °C at 200 V for 4 h. The running buffer was circulated during electrophoresis. Dried gels were exposed to Phosphor Imager screens.

RESULTS

2AP Fluorescence Quenching Is Specific to SAM Binding. Adenine and 2AP have been shown to form isosteric base pairs with thymine (*30*), and it is thus expected that the presence of 2AP at position 138 can also interact with U114 through its Watson−Crick face. 2AP fluorescence emission spectra of the fluorescent aptamer were obtained in the presence of 10 mM $MgCl_2$ (Figure 2A). Upon excitation of 2AP, a relatively high fluorescence was observed, indicating that 2AP is exposed to the solvent, consistent with an unfolded core domain. However, in the presence of SAM, the fluorescence was significantly decreased, indicating that 2AP is internalized in the core region upon SAM binding (Figure 2A, inset). Fluorescence changes were calculated for each SAM concentration and normalized to the fluorescence observed in the absence of ligand. Data were well fitted by a two-state binding model, and a folding transition is observed with an apparent dissociation constant $K_{Dapp} = 5.3 \pm 0.8$ nM (Figure 2A and Table 1). These results are in excellent agreement with previous in-line probing experiments (*6*) in which a dissociation constant of ∼4 nM was determined, indicative of a strong ligand binding affinity as generally observed for natural riboswitches.

For any given genetic switch, the ligand-induced biological response must show a high level of molecular discrimination against closely related analogues. For instance, it has been shown using in-line probing assays that the SAM aptamer exhibits ∼100-fold discrimination against SAH, which only differs from SAM by a single methyl group on the methionine moiety (*6*). An SAH titration was thus performed using the fluorescent aptamer and revealed that 2AP fluorescence quenching does not occur to a significant level (Figure 2A), indicating that the fluorescence quenching is specific to SAM binding, in agreement with in-line probing studies (*6*).

The ion-induced folding of the aptamer may be followed by monitoring the change in fluorescence as a function of magnesium ion concentration. A magnesium titration was performed in the presence of 2 μM SAM, and the data were fitted to a simple two-state model assuming an all-or-none conformational transition induced by the binding of magnesium ions (*22*), with a Hill coefficient *n* and the magnesium

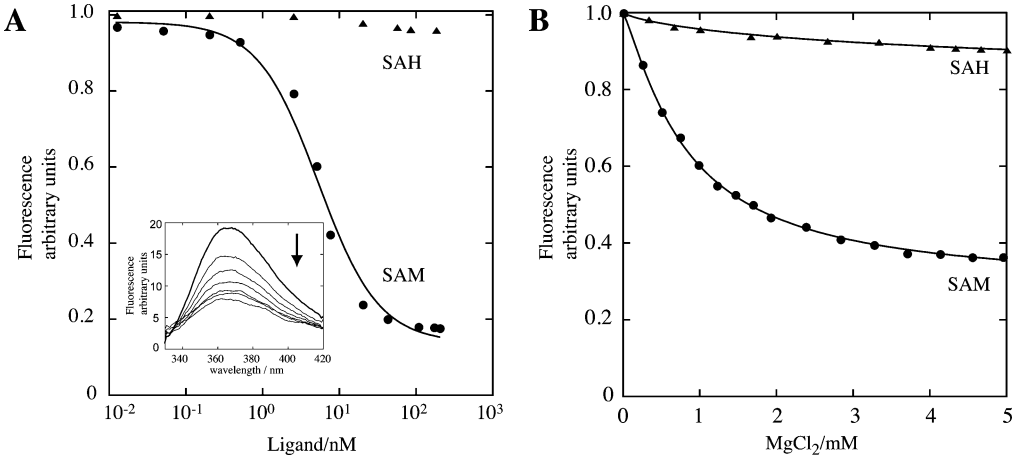

FIGURE 2: 2AP fluorescence is modulated by the specific binding of SAM. (A) Normalized 2AP fluorescence intensity plotted as a function of ligand concentration. Changes of fluorescence were normalized to the maximum fluorescence measured in the absence of ligand. Ligand titrations were performed in the presence of SAM (circles) or SAH (triangles), and lines show the best fits to a binding model (see the Materials and Methods). The inset shows fluorescence emission spectra ($\lambda_{ex} = 300$ nm) from 330 to 420 nm for each SAM concentration. The arrow indicates the decreasing fluorescence due to SAM binding. (B) Folding of the riboswitch aptamer as a function of magnesium ion concentration. Conformational transitions were studied by the normalized change of 2AP fluorescence in the presence of SAM (circles) and SAH (triangles). Experimental data were fitted in each case by regression to a simple two-state model where the binding of metal ions to the aptamer induces a structural change.

Table 1: Ligand Titrations for Various SAM Aptamers[a]

variant	K_{Dapp} (nM)	variant	K_{Dapp} (nM)
WT	5.3 ± 0.8	comp	5.5 ± 0.7
P2	54 ± 5.4	Kt′	47 ± 7.8
core	69 ± 5.9		

[a] Dissociation constants were measured under standard conditions. Asymptotic standard deviations on the fits indicate that errors in K_{Dapp} are generally less than 15% of the values.

ion concentration ($[Mg^{2+}]_{1/2}$) at which the transition is 50% complete. Good fits were obtained with this model, giving values of $n = 1.2 \pm 0.1$ and $[Mg^{2+}]_{1/2} = 0.83$ mM. These values indicate that the SAM-induced 2AP fluorescence quenching is performed by the binding of magnesium ions occurring in the low millimolar range, which is characterized by an apparent lack of cooperativity. The experiment was repeated with 10 times less ligand, and similar binding constants were obtained, indicating that measurements were performed under a saturating concentration of ligand (data not shown). Additional magnesium titration performed with SAH instead of SAM gave values of $n = 0.75 \pm 0.2$ and $[Mg^{2+}]_{1/2} = 5.7$ mM (Figure 2B), indicating that the poor ability of SAH to reorganize the core region cannot be compensated by elevated magnesium ion concentrations (relative to the SAM-bound complex of this investigation).

The Formation of the Pseudoknot Influences the Folding of the Core Region through SAM Binding. A previous study has shown that sequences involved in the SAM riboswitch pseudoknot are important in riboswitch function and proposed that they may interact structurally (*7*), which was further demonstrated in the SAM aptamer crystal structure (*10*). The influence of the pseudoknot on core folding was assessed using 2AP fluorescence assays in conjunction with site-directed mutational analysis. A first mutant was engineered in which guanines 55 and 56 were replaced by cytosines (P2 mutant). A SAM titration experiment showed very low fluorescence quenching (Figure 3A), indicating that the core region of the aptamer is not reorganized to a high degree. 2AP fluorescence data were fitted, and a $K_{Dapp} = 54 \pm 5.4$ nM was obtained. This affinity decrease of 10-fold is consistent with the hypothesis that a compromised pseudoknot markedly affects the SAM-dependent 2AP fluorescence quenching. In addition, the pseudoknot was destabilized by introducing a mutation in the J3/4 single-stranded region where cytosines 115 and 116 were replaced by guanines (core mutant). As observed for the P2 mutant, titration of the SAM metabolite using the core mutant yielded very poor 2AP fluorescence quenching activity, with a $K_{Dapp} = 69 \pm 6.9$ nM. In addition, we generated a compensatory mutant in which both P2 and core mutations were introduced (comp mutant). In contrast to the previous results obtained with the P2 and core mutants, titration of the SAM ligand yielded a large decrease in 2AP fluorescence, indicating the efficient reorganization of the core region of the aptamer. A fitted value of $K_{Dapp} = 5.5 \pm 0.7$ nM was calculated representing an affinity similar to the one observed for the natural sequence. The result obtained with the comp mutant indicates that formation of the pseudoknot is possible as long as the base pairing potential is maintained and that pseudoknot formation is important for the ligand-induced folding of the core region.

The Pseudoknot Is Important for the Global Folding of the Aptamer. The previous SAM and magnesium ion titrations show that the pseudoknot-dependent core reorganization is achieved when SAM binding occurs. Although these results clearly indicate that the pseudoknot is important for ligand binding, they do not provide information about pseudoknot formation in the absence of ligand. To determine whether this tertiary structure is dependent upon ligand binding, we monitored the formation of the pseudoknot using a native gel assay. This technique has been successfully used to study global conformational changes in nucleic acids given that a compact structure generally migrates faster than a more extended one (*31*−*36*). We reasoned that aptamers in which the pseudoknot is formed should have a more compact structure than aptamers such as the P2 mutant, which are compromised in the pseudoknot formation, and should

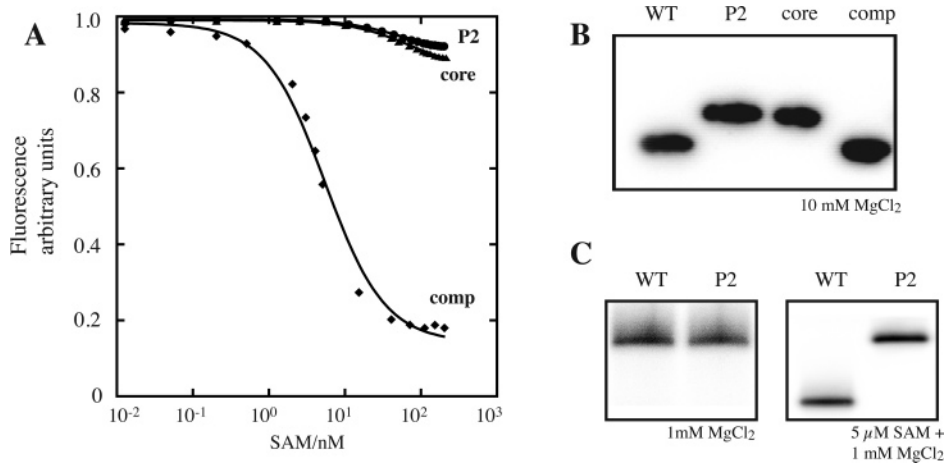

FIGURE 3: Role of the pseudoknot in aptamer core folding. (A) Normalized 2AP fluorescence intensity plotted as a function of SAM concentration. SAM titrations were performed using aptamers with pseudoknot-disruptive mutations in the P2 (circles) and core (triangles) regions and also with an aptamer having compensatory mutations (tilted squares). (B) Nondenaturing gel electrophoresis of the wild type (WT) and three SAM aptamer mutants in the presence of 10 mM magnesium. P2 and core mutants exhibit retarded electrophoretic mobilities, while the mobility is largely restored for the compensatory mutant (comp). (C) Nondenaturing gel electrophoresis performed under low magnesium concentrations (e.g., 1 mM) in the absence (left panel) or in the presence (right panel) of 5 μM SAM for WT and P2 aptamers. From the migration profiles, it is apparent that SAM binding to the WT molecule is associated with the adoption of a more compact aptamer molecule.

therefore display a faster migration rate. A representative gel performed in the presence of 10 mM magnesium ions (Figure 3B) shows that the gel migration pattern of the wild-type aptamer displays a unique band, indicating that it is folded as a homogeneous species. The migration pattern of the P2 mutant also shows a unique species but exhibits a slower migration rate, suggesting the adoption of an extended structure, indicative of its inability to form a pseudoknot. Similarly, the core mutant displayed a slow migration, also indicative of its reduced ability to form a pseudoknot. However, when the interaction was re-established (comp mutant), a migration pattern similar to that of the wild type was observed, suggesting that pseudoknot formation can occur as long as base pairing potential is maintained, which is in agreement with a previous study (*7*).

To determine whether SAM binding also influences the global structure of the aptamer, we repeated the native gel electrophoresis experiment in the presence of a lower magnesium ion concentration (e.g., 1 mM). In these conditions, the electrophoretic mobilities of both wild-type and P2 mutant molecules are very similar, indicating that they adopt an extended structure (Figure 3C, left). However, upon addition of 5 μM SAM, the migration rate of the wild-type molecule is markedly faster than that of the P2 mutant, suggesting that SAM binding to the wild-type molecule promotes compaction of the global structure (Figure 3C, right). These results show that, in addition to reorganizing the core region, SAM binding also favors the formation of a compact structure which depends on the presence of a functional pseudoknot. Recently, a similar ligand-induced compaction was observed in the glycine riboswitch tandem aptamer, which was characterized using hydroxyl radical footprinting and small-angle X-ray scattering (SAXS) (*37*).

B. subtilis SAM Aptamers Exhibit an Unconventional K-Turn Consensus Sequence. Upon examining the secondary structure of the aptamer (Figure 1A), it is apparent that the P2 helical domain contains a bubble region bearing structural similarities to a K-turn motif, which is known to introduce a tight kink into the helical axis (*14*). The conventional K-turn secondary structure representation is shown in Figure 4A. Although the K-turn sequence found in the *yitJ* SAM aptamer is closely similar to the K-turn consensus (Figure 4A) (*14*), the C58−G50 base pair of *yitJ* differs from the consensus sequence since it is reversed in the latter (Figure 4A). This difference prompted us to verify whether the *yitJ* K-turn motif behaves as a typical one. For instance, because of its location in the P2 helical domain, it is expected that the correct folding of the K-turn should be required for pseudoknot formation. A native gel assay was thus used in which a K-turn-deficient molecule (Kt′ mutant; A48C) was studied in comparison to the wild-type molecule (Figure 4B). From the migration profile, it is apparent that the Kt′ variant is significantly retarded compared to the wild-type molecule, supporting the hypothesis that the K-turn is important for the formation of the pseudoknot.

We also verified whether the *yitJ* K-turn motif is able to bind the L7Ae protein, which is known to bind a K-turn element in a box C/D RNA and to induce its folding into a tightly kinked conformation (*16*, *29*). A gel electrophoretic retardation assay was used to monitor the formation of a complex between the wild-type SAM aptamer and L7Ae. Our analysis shows that two species corresponding to the free and L7Ae-bound aptamers are detected (Figure 4C). To determine whether L7Ae binding is dependent upon pseudoknot formation, the same experiment was repeated using a P2 mutant. Although the migration profile is consistent with that of a slower migrating pseudoknot-deficient molecule, RNA−protein complex formation is still observed, suggesting that folding of the K-turn motif remains unaltered by pseudoknot disruption. However, to ascertain that L7Ae binding occurs specifically through the K-turn motif, a negative control was performed in which the Kt′ mutant was used to preclude L7Ae binding to the K-turn domain of the SAM aptamer. Similar to the P2 mutant, a slow migration profile indicating the absence of pseudoknot formation was observed, but for which no aptamer−L7Ae complex was formed, consistent with the idea that L7Ae must bind the SAM aptamer via the K-turn motif (Figure 4C).

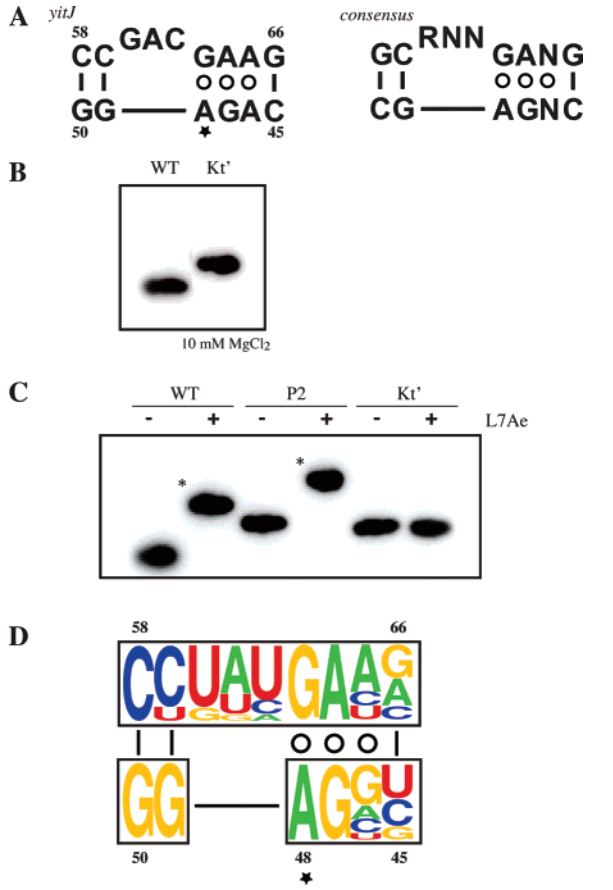

FIGURE 4: Role of the K-turn motif in aptamer global structure. (A) Secondary structures for the *yitJ* (left) and the reported consensus (right) (*14*) K-turn motifs. The asterisk shows nucleotide A48 known to be important for the adoption of the K-turn structure in Kt-7 (*17*). Watson−Crick and heteropurine base pairs are represented by lines and circles, respectively. R stands for purine. (B) Nondenaturing gel electrophoresis of the WT and Kt′ mutant (A48C) in the presence of 10 mM magnesium. Disruption of the K-turn motif produces slower migration, consistent with the apparent absence of pseudoknot formation. (C) Gel mobility shift assay of SAM aptamers with and without the L7Ae protein. While the K-turn binding L7Ae protein can perform RNA−protein complexes with WT and P2 mutant molecules, no interaction is observed when using an aptamer containing an inactivated K-turn motif (Kt′ mutant). The RNA−protein complex is indicated by an asterisk. The migration profile of free and bound WT species is faster than that of P2 and Kt′ aptamers due to a compact fold. (D) Graphical representation of a K-turn motif generated from 11 SAM aptamer sequences found in *B. subtilis*. A proportional representation for each residue is shown. The logo is arranged to match the secondary structure of the K-turn. Nucleotide positions are indicated below each representation, and an asterisk indicates the location of A48.

Using the WebLogo application (*38*), 11 K-turn sequences found in *B. subtilis* SAM aptamers were used to generate a graphical representation of the K-turn motif (Figure 4D). Strongly conserved sequence elements can be observed corresponding to distal base pairs (G49−C59 and G50−C58). Thus, the G50−C58 base pair, which is different from the original K-turn consensus (*14*), is not particular to the *yitJ* sequence but is conserved in all SAM aptamers. Moreover, the unpaired region which corresponds to positions 60−62 does not conform to the consensus sequence (RNN) given that the UAU sequence is the most represented one (Figure 4D). Thus, K-turn structures present in SAM aptamers differ from the originally proposed K-turn motif, suggesting that K-turn structures can most probably be formed from a greater number of sequences than originally conceived, as observed in a recent study (*39*).

The K-Turn Motif Is Important for the Folding of the Core Domain. The K-turn motif is located in the middle of the P2 helical domain, which is involved in the formation of the pseudoknot. We speculated that because aptamers having an altered K-turn motif do not allow the formation of the pseudoknot, they should exhibit a low fluorescence quenching upon ligand binding, reflecting the decreased propensity of the core domain to be reorganized. An aptamer variant was generated in which an A48C mutation was introduced to inhibit the adoption of the K-turn structure (Kt′ mutant), and as expected, upon titration of SAM, a low 2AP fluorescence quenching was observed (Figure 5A). The fluorescence data were fitted, and a K_{Dapp} of 47 ± 7.8 nM was calculated corresponding to an affinity decrease of ~8-fold. This result indicates that the K-turn structure is important for ligand binding, which in turn plays a major role in the core reorganization of the aptamer domain. Also, because L7Ae has been shown to induce the folding of a K-turn motif (*29*), we reasoned that L7Ae binding to the SAM aptamer could promote formation of the ligand−aptamer complex by stabilizing the K-turn structure, which would suggest that proteins could be involved in the folding of K-turn-containing riboswitch mRNA molecules. The ion-induced folding of the aptamer variant was thus performed in the presence of 1 μM L7Ae (Figure 5B), and values of $n = 1.5 \pm 0.1$ and $[Mg^{2+}]_{1/2} = 0.11$ mM were obtained, indicating an important stabilizing effect of 7.5-fold on the formation of the ligand−aptamer complex. No such change could be detected when the same experiment was performed using the Kt′ mutant ($n = 1.3 \pm 0.1$ and $[Mg^{2+}]_{1/2} = 0.79$ mM), suggesting that the effect is not caused by a direct fluorescence quenching of the protein on 2AP (Figure 5B). These results strongly support the hypothesis that L7Ae binding to the SAM aptamer promotes ligand binding by stabilizing the K-turn structure.

DISCUSSION

The SAM riboswitch is the only one for which at least three structurally different aptamers are known to specifically recognize the same ligand, suggesting that nature can satisfactorily find different RNA structure solutions for a given molecular recognition challenge (*6*, *9*, *40*). Thus, the variety of naturally occurring SAM-sensing aptamers constitutes a fantastic opportunity to unravel how RNA molecules perform specific ligand recognition only using a handful of functional groups when compared to their protein counterparts. This work was aimed at characterizing the structural changes experienced by the SAM riboswitch class I aptamer in the presence of SAM in an attempt to understand the functional implications of peripheral elements on the ligand binding site.

Given that it was previously observed using in-line probing that the core region of the aptamer is reorganized upon SAM binding (*6*), we introduced a fluorescent 2AP local reporter in the core aptamer domain at position 138 to monitor ligand-induced structural changes. According to the crystal structure (*10*), the (A138−U114)·A52 triple is important to tie the P1−P4 helical stack to the pseudoknot. Our results are

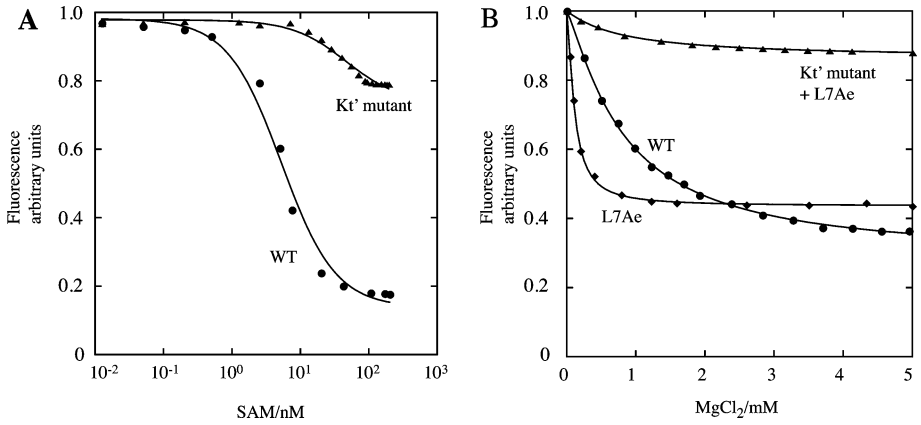

FIGURE 5: Role of K-turn formation in SAM-dependent 2AP fluorescence quenching. (A) Normalized 2AP fluorescence intensity plotted as a function of SAM concentration. SAM titrations were performed using the wild-type (circles) or the Kt′ mutant (triangles) aptamers. Disruption of the K-turn motif markedly influences the core domain reorganization. (B) Normalized 2AP fluorescence intensity for the wild-type aptamer in the absence (circles) or in the presence of L7Ae (tilted squares) and for the Kt′ mutant in the presence of L7Ae (circles) as a function of magnesium ion concentration. The presence of L7Ae markedly promotes the formation of the aptamer−SAM complex. Lines show the best fits to a stoichiometric binding model.

consistent with a model in which the local environment of the (A138−U114)·A52 triple is modulated in the presence of SAM, which could be important for the P1−P4 helical stacking and thus for the global folding of the SAM aptamer domain. However, because 2AP fluorescence quenching is mainly caused by stacking interactions with no significant contribution from base-pairing or hydrogen-bonding (*41*), our results do not provide information on the actual formation of the U114−A138 Watson−Crick base pair, which could form either prior to or during the ligand binding step. Nevertheless, as we and others have found in previous studies of the adenine riboswitch aptamer (*35*, *36*, *42*, *43*), 2AP fluorescence is a useful tool for monitoring local structural changes that can, as found here, be modulated by the presence of a target ligand.

The SAM aptamer domain is organized around a typical four-way junction containing a tertiary pseudoknot interaction, which was previously shown to be important for riboswitch transcriptional control (*7*). Our results show that formation of this tertiary interaction is very important for the ligand-induced core reorganization as disruption of either region markedly decreases SAM-dependent fluorescence quenching (Figure 3A). Moreover, our results suggest that pseudoknot formation can occur in absence of SAM (Figure 3B) and also that, in a lower magnesium concentration, SAM binding is required for a pseudoknot-dependent global reorganization to take place (Figure 3C). Interestingly, a recent study has shown that the related *ykrW* SAM binding domain exhibits a pseudoknot that is dependent on the presence of SAM (*7*). Visual inspection of both *yitJ* and *ykrW* secondary structures suggests that the latter may have weaker base pairs that are involved in the pseudoknot and could provide a structural basis for the requirement of SAM binding for the formation of the pseudoknot. The functional implications for aptamers having a pseudoknot that forms in the absence of the ligand could lie in an increased ligand binding affinity given that the pseudoknot structure most probably stabilizes the ligand−aptamer complex.

The pseudoknot interaction can be viewed as an auxiliary folding element which is intimately linked to the adoption of the native structure of the SAM aptamer. A similar situation is present in the very well-characterized four-way junction hairpin ribozyme, in which a long-range tertiary interaction is made by bubble regions (loops A and B) located in two adjacent arms (*44*, *45*). The loop A−loop B interaction also contains a very important tertiary Watson−Crick interaction involving a guanine immediately adjacent to the cleavage site (*46*), which has been observed in the crystal structure and suggested to be important for the in-line arrangement of the nucleophile and leaving group (*47*). In the context of the SAM riboswitch aptamer, formation of Watson−Crick base pairs in the core region, immediately adjacent to U114, are most probably important to accommodate formation of a U114−A138 base pair and the concurrent reorganization of the core domain. This is particularly clear from the very low 2AP fluorescence quenching activity of pseudoknot-inactive aptamers (P2 and core mutants), which suggests that the pseudoknot interaction is important for the ligand binding site formation. Moreover, in the lysine riboswitch aptamer, a related peripheral loop−loop element predicted to occur between two adjacent loops (*48*, *49*) was recently confirmed by us (*50*), for which we also demonstrated the importance in the lysine riboswitch gene regulation control. However, in contrast to what we report here for the SAM riboswitch, the inhibition of the lysine aptamer loop−loop interaction results in a decrease in ligand binding affinity rather than a complete inability to bind the ligand. This could be explained by the fact that both elements participating in the tertiary interaction in the lysine aptamer are located outside of the ligand-induced reorganized region (*51*) and are not directly involved in the formation of the ligand binding site. This case is reminiscent of the adenine riboswitch for which we have recently shown that ligand binding can occur prior to formation of the loop−loop interaction (*36*).

The formation of the SAM aptamer pseudoknot interaction is characterized by a faster migration rate in native gels (Figure 3B). This faster migration can be explained by the adoption of a more compact structure in the presence of the pseudoknot. We recently reported a similar situation for the adenine riboswitch where the formation of the loop−loop interaction is associated with a faster migration in native gel electrophoresis (*35*, *36*). However, in contrast to these studies, we observe for the SAM riboswitch aptamer that

structure compaction can also be promoted by ligand binding (Figure 3C) and that it is strongly dependent upon formation of the pseudoknot, most probably because of its requirement for ligand binding in a low magnesium concentration (*7*). SAXS analysis of the glycine riboswitch aptamer has identified structural conformations corresponding to an unfolded state in the absence of magnesium ions and ligand and to folded states in the presence of magnesium ions and ligand, where each added cofactor resulted in the compaction of the RNA molecule as measured by diminution of the radius of gyration (R_g) as well as molecular envelope restoration (*37*). In addition, a thi-box riboswitch has recently been shown by crystallography to undergo local compaction upon binding to its cognate ligand (*52*). Thus, ligand-induced compaction of riboswitch aptamers may be a salient feature of several riboswitches and may have important implications for the riboswitch regulatory activity such as the stabilization of the aptamer when bound to its ligand. Consistent with this interpretation, we have previously shown by single-molecule FRET that ligand binding to the aptamer of the adenine riboswitch results in a 10-fold decrease in the folding heterogeneity of the loop−loop interaction, consistent with ligand-induced stabilization of this RNA structure (*36*).

The SAM aptamer K-turn motif is located between two regions that are involved in the formation of the pseudoknot, and it is highly probable that the sharp kink that it introduces is important for this tertiary structure to take place. This is emphasized by nondenaturing gel experiments in which disruption of the K-turn motif prevents formation of the pseudoknot (Figure 4B), which in turn is reflected by the reduced ligand-induced core reorganization (Figure 5A). Thus, our results show that the presence of the K-turn element in the context of the S box is important for the correct folding of the aptamer and for efficient ligand binding. Its importance was also previously shown in transcriptional regulation using in vivo reporter gene assays (*11*). Interestingly, most of the K-turn sequences present in *B. subtilis* SAM aptamers do not conform to the K-turn consensus previously reported by Steitz and co-workers (*14*). For instance, the three-nucleotide single-stranded region of the consensus is RNN (R = purine), while the most represented sequence in *B. subtilis* SAM aptamers corresponds to UAU (Figure 4D), suggesting that the number of sequences able to adopt a K-turn motif is broader than previously suggested. A recent study using isostericity matrices for deriving sequence signatures of recurrent motifs has identified several K-turn candidates which deviate from the proposed consensus but that display tertiary structure highly similar to that of an archetypal K-turn (*39*). Another example of the molecular flexibility exhibited by K-turn domains is well represented by K-loop motifs, which indicate that K-turn binding proteins may only require heteropurine pairs for RNA−protein complex formation (*53*, *54*). Thus, continued efforts to generate crystallographic structures of K-turn-containing RNA molecules should provide insights into the rules that govern K-turn structural folding.

K-turn motifs occur in several domains of the 23S rRNA as observed in the large ribosomal subunit crystal structure (*12*, *14*). One of them, Kt-7, is located in the context of a three-way RNA junction, called 5−6−7, which exhibits a loop−loop interaction (*12*). Interestingly, the K-turn motif is located in one of the arms that participate in the loop−loop interaction. This suggests that the role of the K-turn structure in the architectural arrangement of the 5−6−7 junction is to provide a structural bend allowing formation of the loop−loop interaction. In addition, another similar arrangement is proposed to reside in the lysine riboswitch (*48*). Visual inspection of the secondary structure of the lysine-sensing domain indicates that a K-turn is present in one of the arms involved in the loop−loop interaction. We have shown the importance of this K-turn motif in providing the required structural bend necessary for the tertiary interaction to occur (*50*). The K-turn, being a structural facilitator to form higher order structural arrangements, plays a very similar role in the SAM riboswitch aptamer. Because the formation of the pseudoknot is essential for ligand binding and its formation depends on the folding of the K-turn, it is expected that the folding of the latter is intimately linked with the binding activity of the SAM riboswitch aptamer. In a recent FRET study, the $[Mg^{2+}]_{1/2}$ required for the folding of an isolated K-turn domain was found to be 1 mM (*17*). This Mg^{2+} concentration is in a range similar to that observed for the SAM-induced 2AP fluorescence quenching (0.83 mM), suggesting a concomitant folding of the K-turn motif and the entire SAM aptamer. Interestingly, stabilization of the K-turn by the L7Ae protein promotes SAM binding as observed by a lower $[Mg^{2+}]_{1/2}$ value of 0.11 mM obtained in the presence of the protein. These results are consistent with the idea that the folding of the K-turn motif is important in the preorganization of the ligand binding site, the latter being further rearranged upon ligand binding as shown by in-line probing experiments (*6*). Thus, the implication of the K-turn motif as a pseudoknot facilitator is consistent with the proposal that there are a limited number of RNA structural motifs that constitute the majority of building blocks used in the arrangement of relatively complex RNA molecules (*55*, *56*).

The positive influence of the L7Ae protein on the formation of the ligand−aptamer complex raises some interesting questions about potential roles that L7Ae proteins could exert on riboswitches in vivo. For instance, our results are in agreement with the idea that protein binding could potentially fine-tune SAM riboswitch activity to be more sensitive to metabolites. However, from minimally reconstituted transcription and translation systems, riboswitches are considered to perform their regulation without the aid of protein cofactors, suggestive of a very ancient regulation system (*56*). A possible evolutionary scenario for this RNA-based gene regulation system could be that proteins have been involved as auxiliary folding factors by stabilizing specific RNA structures at some point during evolution. It is interesting to note that ribosomal proteins bearing structural similarities to L7Ae are present in some representatives of *Bacillus* (e.g., *Bacillus halodurans*). Similar hypotheses are considered for group II intron and RNase P ribozymes where many variants have lost the ability to function autonomously, possibly as a result of an evolutionary process where the loss of activity was compensated by the recruitment of protein cofactors (*57*, *58*). One of the most striking examples of this is found in the ribosome, which has been shown to be a ribozyme (*59*), where the crystal structure of the large ribosomal subunit of the *Haloarcula marismortui* shows that most proteins stabilize the structure by interacting with several RNA domains, some of them being K-turn motifs

(*12*). Taken together, these observations suggest that some riboswitches may function with the help of protein cofactors via the use of K-turn motifs as recognition elements. However, it should be emphasized that evidence for in vivo riboswitch−protein complexes has yet to be shown. Nevertheless, a recent study using a bioinformatic approach has identified additional RNA elements sharing characteristics of riboswitch function and suggests an expanded scope for riboswitches in bacterial genetic control (*60*). Such findings provide hints that further types of riboswitches will be uncovered in the future and that perhaps some of them will strictly require protein cofactors to ensure their biological function.

ACKNOWLEDGMENT

We thank Drs. Carlos Penedo and David Norman and members of the Lafontaine laboratory for helpful discussions and Alain Lavigueur for critical reading of the manuscript. We also thank D. M. J. Lilley for the generous gift of the L7Ae protein.

REFERENCES

1. Nudler, E., and Mironov, A. S. (2004) The riboswitch control of bacterial metabolism, *Trends Biochem. Sci. 29*, 11−7.
2. Grundy, F. J., and Henkin, T. M. (1998) The S box regulon: a new global transcription termination control system for methionine and cysteine biosynthesis genes in gram-positive bacteria, *Mol. Microbiol. 30*, 737−49.
3. Yocum, R. R., Perkins, J. B., Howitt, C. L., and Pero, J. (1996) Cloning and characterization of the metE gene encoding S-adenosylmethionine synthetase from Bacillus subtilis, *J. Bacteriol. 178*, 4604−10.
4. McDaniel, B. A., Grundy, F. J., Artsimovitch, I., and Henkin, T. M. (2003) Transcription termination control of the S box system: direct measurement of S-adenosylmethionine by the leader RNA, *Proc. Natl. Acad. Sci. U.S.A. 100*, 3083−8.
5. Epshtein, V., Mironov, A. S., and Nudler, E. (2003) The riboswitch-mediated control of sulfur metabolism in bacteria, *Proc. Natl. Acad. Sci. U.S.A. 100*, 5052−6.
6. Winkler, W. C., Nahvi, A., Sudarsan, N., Barrick, J. E., and Breaker, R. R. (2003) An mRNA structure that controls gene expression by binding S-adenosylmethionine, *Nat. Struct. Biol. 10*, 701−7.
7. McDaniel, B. A., Grundy, F. J., and Henkin, T. M. (2005) A tertiary structural element in S box leader RNAs is required for S-adenosylmethionine-directed transcription termination, *Mol. Microbiol. 57*, 1008−21.
8. Lim, J., Winkler, W. C., Nakamura, S., Scott, V., and Breaker, R. R. (2006) Molecular-recognition characteristics of SAM-binding riboswitches, *Angew. Chem., Int. Ed. Engl. 45*, 964−8.
9. Corbino, K. A., Barrick, J. E., Lim, J., Welz, R., Tucker, B. J., Puskarz, I., Mandal, M., Rudnick, N. D., and Breaker, R. R. (2005) Evidence for a second class of S-adenosylmethionine riboswitches and other regulatory RNA motifs in alpha-proteobacteria, *Genome Biol. 6*, R70.
10. Montange, R. K., and Batey, R. T. (2006) Structure of the S-adenosylmethionine riboswitch regulatory mRNA element, *Nature 441*, 1172−5.
11. Winkler, W. C., Grundy, F. J., Murphy, B. A., and Henkin, T. M. (2001) The GA motif: an RNA element common to bacterial antitermination systems, rRNA, and eukaryotic RNAs, *RNA 7*, 1165−72.
12. Ban, N., Nissen, P., Hansen, J., Moore, P. B., and Steitz, T. A. (2000) The complete atomic structure of the large ribosomal subunit at 2.4 A resolution, *Science 289*, 905−20.
13. Schluenzen, F., Tocilj, A., Zarivach, R., Harms, J., Gluehmann, M., Janell, D., Bashan, A., Bartels, H., Agmon, I., Franceschi, F., and Yonath, A. (2000) Structure of functionally activated small ribosomal subunit at 3.3 angstroms resolution, *Cell 102*, 615−23.
14. Klein, D. J., Schmeing, T. M., Moore, P. B., and Steitz, T. A. (2001) The kink-turn: a new RNA secondary structure motif, *EMBO J. 20*, 4214−21.
15. Vidovic, I., Nottrott, S., Hartmuth, K., Luhrmann, R., and Ficner, R. (2000) Crystal structure of the spliceosomal 15.5kD protein bound to a U4 snRNA fragment, *Mol. Cell 6*, 1331−42.
16. Moore, T., Zhang, Y., Fenley, M. O., and Li, H. (2004) Molecular basis of box C/D RNA-protein interactions; cocrystal structure of archaeal L7Ae and a box C/D RNA, *Structure 12*, 807−18.
17. Goody, T. A., Melcher, S. E., Norman, D. G., and Lilley, D. M. (2004) The kink-turn motif in RNA is dimorphic, and metal ion-dependent, *RNA 10*, 254−64.
18. Ward, D. C., Reich, E., and Stryer, L. (1969) Fluorescence studies of nucleotides and polynucleotides. I. Formycin, 2-aminopurine riboside, 2,6-diaminopurine riboside, and their derivatives, *J. Biol. Chem. 244*, 1228−37.
19. Xu, D., Evans, K. O., and Nordlund, T. M. (1994) Melting and premelting transitions of an oligomer measured by DNA base fluorescence and absorption, *Biochemistry 33*, 9592−9.
20. Stivers, J. T. (1998) 2-Aminopurine fluorescence studies of base stacking interactions at abasic sites in DNA: metal-ion and base sequence effects, *Nucleic Acids Res. 26*, 3837−44.
21. Jean, J. M., and Hall, K. B. (2001) 2-Aminopurine fluorescence quenching and lifetimes: role of base stacking, *Proc. Natl. Acad. Sci. U.S.A. 98*, 37−41.
22. Lafontaine, D. A., Wilson, T. J., Zhao, Z. Y., and Lilley, D. M. (2002) Functional group requirements in the probable active site of the VS ribozyme, *J. Mol. Biol. 323*, 23−34.
23. Declais, A. C., and Lilley, D. M. (2000) Extensive central disruption of a four-way junction on binding CCE1 resolving enzyme, *J. Mol. Biol. 296*, 421−33.
24. Milligan, J. F., Groebe, D. R., Witherell, G. W., and Uhlenbeck, O. C. (1987) Oligoribonucleotide synthesis using T7 RNA polymerase and synthetic DNA templates, *Nucleic Acids Res. 15*, 8783−98.
25. Pleiss, J. A., Derrick, M. L., and Uhlenbeck, O. C. (1998) T7 RNA polymerase produces 5′ end heterogeneity during in vitro transcription from certain templates, *RNA 4*, 1313−7.
26. Wilson, T. J., and Lilley, D. M. (2002) Metal ion binding and the folding of the hairpin ribozyme, *RNA 8*, 587−600.
27. Flannery, B. P., Teukolsky, S. A., and Vetterling, W. T. (1992) *Numerical Recipes in Fortran*, 2nd ed., Cambridge University Press, Cambridge, U.K.
28. Rist, M., and Marino, J. (2001) Association of an RNA kissing complex analyzed using 2-aminopurine fluorescence, *Nucleic Acids Res. 29*, 2401−8.
29. Turner, B., Melcher, S. E., Wilson, T. J., Norman, D. G., and Lilley, D. M. (2005) Induced fit of RNA on binding the L7Ae protein to the kink-turn motif, *RNA 11*, 1192−200.
30. Law, S. M., Eritja, R., Goodman, M. F., and Breslauer, K. J. (1996) Spectroscopic and calorimetric characterizations of DNA duplexes containing 2-aminopurine, *Biochemistry 35*, 12329−37.
31. Lilley, D. M. (1998) Folding of branched RNA species, *Biopolymers 48*, 101−112.
32. Silverman, S. K., and Cech, T. R. (1999) Energetics and cooperativity of tertiary hydrogen bonds in RNA structure, *Biochemistry 38*, 8691−702.
33. Silverman, S. K., Zheng, M., Wu, M., Tinoco, I. Jr., and Cech, T. R. (1999) Quantifying the energetic interplay of RNA tertiary and secondary structure interactions, *RNA 5*, 1665−74.
34. Yamauchi, T., Miyoshi, D., Kubodera, T., Nishimura, A., Nakai, S., and Sugimoto, N. (2005) Roles of Mg(2+) in TPP-dependent riboswitch, *FEBS Lett. 579*, 2583−2588.
35. Lemay, J. F., and Lafontaine, D. A. (2007) Core requirements of the adenine riboswitch aptamer for ligand binding, *RNA 13*, 339−50.
36. Lemay, J. F., Penedo, J. C., Tremblay, R., Lilley, D. M., and Lafontaine, D. A. (2006) Folding of the adenine riboswitch, *Chem. Biol. 13*, 857−68.
37. Lipfert, J., Das, R., Chu, V. B., Kudaravalli, M., Boyd, N., Herschlag, D., and Doniach, S. (2007) Structural transitions and thermodynamics of a glycine-dependent riboswitch from Vibrio cholerae, *J. Mol. Biol. 365*, 1393−406.
38. Crooks, G. E., Hon, G., Chandonia, J. M., and Brenner, S. E. (2004) WebLogo: a sequence logo generator, *Genome Res. 14*, 1188−90.
39. Lescoute, A., Leontis, N. B., Massire, C., and Westhof, E. (2005) Recurrent structural RNA motifs, isostericity matrices and sequence alignments, *Nucleic Acids Res. 33*, 2395−409.

40. Fuchs, R. T., Grundy, F. J., and Henkin, T. M. (2006) The S(MK) box is a new SAM-binding RNA for translational regulation of SAM synthetase, *Nat. Struct. Mol. Biol. 13*, 226−33.
41. Rachofsky, E. L., Osman, R., and Ross, J. B. (2001) Probing structure and dynamics of DNA with 2-aminopurine: effects of local environment on fluorescence, *Biochemistry 40*, 946−56.
42. Gilbert, S. D., Stoddard, C. D., Wise, S. J., and Batey, R. T. (2006) Thermodynamic and kinetic characterization of ligand binding to the purine riboswitch aptamer domain, *J. Mol. Biol. 359*, 754−768.
43. Rieder, R., Lang, K., Graber, D., and Micura, R. (2007) Ligand-induced folding of the adenosine deaminase A-riboswitch and implications on riboswitch translational control, *ChemBioChem 8*, 896−902.
44. Murchie, A. I., Thomson, J. B., Walter, F., and Lilley, D. M. (1998) Folding of the hairpin ribozyme in its natural conformation achieves close physical proximity of the loops, *Mol. Cell 1*, 873−81.
45. Walter, N. G., Burke, J. M., and Millar, D. P. (1999) Stability of hairpin ribozyme tertiary structure is governed by the interdomain junction. *Nat. Struct. Biol. 6*, 544−9.
46. Pinard, R., Lambert, D., Walter, N. G., Heckman, J. E., Major, F., and Burke, J. M. (1999) Structural basis for the guanosine requirement of the hairpin ribozyme, *Biochemistry 38*, 16035−9.
47. Rupert, P. B., and Ferre-D'Amare, A. R. (2001) Crystal structure of a hairpin ribozyme-inhibitor complex with implications for catalysis, *Nature 410*, 780−6.
48. Grundy, F. J., Lehman, S. C., and Henkin, T. M. (2003) The L box regulon: lysine sensing by leader RNAs of bacterial lysine biosynthesis genes, *Proc. Natl. Acad. Sci. U.S.A. 100*, 12057−62.
49. Rodionov, D. A., Vitreschak, A. G., Mironov, A. A., and Gelfand, M. S. (2003) Regulation of lysine biosynthesis and transport genes in bacteria: yet another RNA riboswitch, *Nucleic Acids Res. 31*, 6748−57.
50. Blouin, S., and Lafontaine, D. A. (2007) A loop-loop interaction and a K-turn motif located in the lysine aptamer domain are important for the riboswitch gene regulation control, *RNA 13*, 1256−1267.
51. Sudarsan, N., Wickiser, J. K., Nakamura, S., Ebert, M. S., and Breaker, R. R. (2003) An mRNA structure in bacteria that controls gene expression by binding lysine, *Genes Dev. 17*, 2688−97.
52. Edwards, T. E., and Ferre-D'Amare, A. R. (2006) Crystal structures of the thi-box riboswitch bound to thiamine pyrophosphate analogs reveal adaptive RNA-small molecule recognition, *Structure 14*, 1459−68.
53. Hamma, T., and Ferre-D'Amare, A. R. (2004) Structure of protein L7Ae bound to a K-turn derived from an archaeal box H/ACA sRNA at 1.8 A resolution, *Structure 12*, 893−903.
54. Nolivos, S., Carpousis, A. J., and Clouet-d'Orval, B. (2005) The K-loop, a general feature of the Pyrococcus C/D guide RNAs, is an RNA structural motif related to the K-turn, *Nucleic Acids Res. 33*, 6507−14.
55. Moore, P. B. (1999) Structural motifs in RNA, *Annu. Rev. Biochem. 68*, 287−300.
56. Winkler, W. C., and Breaker, R. R. (2005) Regulation of bacterial gene expression by riboswitches, *Annu. Rev. Microbiol. 59*, 487−517.
57. Ostheimer, G. J., Williams-Carrier, R., Belcher, S., Osborne, E., Gierke, J., and Barkan, A. (2003) Group II intron splicing factors derived by diversification of an ancient RNA-binding domain, *EMBO J. 22*, 3919−29.
58. Evans, D., Marquez, S. M., and Pace, N. R. (2006) RNase P: interface of the RNA and protein worlds, *Trends Biochem. Sci. 31*, 7069−7082.
59. Nissen, P., Hansen, J., Ban, N., Moore, P. B., and Steitz, T. A. (2000) The structural basis of ribosome activity in peptide bond synthesis, *Science 289*, 920−30.
60. Barrick, J. E., Corbino, K. A., Winkler, W. C., Nahvi, A., Mandal, M., Collins, J., Lee, M., Roth, A., Sudarsan, N., Jona, I., Wickiser, J. K., and Breaker, R. R. (2004) New RNA motifs suggest an expanded scope for riboswitches in bacterial genetic control, *Proc. Natl. Acad. Sci. U.S.A. 101*, 6421−6.
61. Delano, W. L. (2002) *The PyMOL Molecular Graphics System*, DeLano Scientific, San Carlos, CA.

BI701164Y